

Parameterization of the Stoner-Wohlfarth model of magnetic hysteresis

Nikolai A. Zarkevich,^{1,*} Cajetan Ikenna Nlebedim,^{1,†} and R. William McCallum¹

¹Ames Laboratory, U.S. Department of Energy, Ames, Iowa 50011-3020, USA

(Dated: January 21, 2022)

The Stoner-Wohlfarth is the most used model of magnetic hysteresis, but its computation is time-consuming. We use machine learning to approximate piecewise this model by easy-to-compute analytic functions. Our parametrization is suitable for fast quantitative evaluations and fitting experimental data, which we exemplify.

Keywords: Magnetic hysteresis, Stoner-Wohlfarth, machine learning.

INTRODUCTION

Mathematical models [1, 2], databases [3–5], and machine learning techniques [6–10] are extensively used for materials discovery [11–14]. Known analytical approximations and predictive estimates [15–20] greatly simplify those efforts, especially for magnetic materials [21–25]. There are several competing methods for approximating a function.

1. A smooth function can be approximated by a basis expansion. Examples are a Taylor expansion, a Fourier series, a basis of gaussians, etc.
2. Any piecewise-differentiable function can be approximated piecewise by the rational functions, which may have poles. An example is $1/r$.
3. Any continuous function can be approximated by a deep learning network (DLN), which is not differentiable [26–28].

Preference is given to a more precise approximation with fewer fitted parameters. As a bonus, the rational functions and many analytic basis functions have known derivatives. Thus, for smooth or differentiable functions, methods 1 and 2 are preferable to DLN #3. Combining a functional mapping with method 2, we approximate the Stoner-Wohlfarth (SW) piecewise-differentiable $m(h)$ curve (Fig. 1).

The SW model [1] describes the hysteresis curve [29] for a random distribution of non-interacting uniaxial particles whose magnetization reverses through coherent rotation. It remains the most popular model of magnetic hysteresis for hard magnets [2]. The SW model [1] presents the magnetization curve $m(h)$ in terms of the reduced magnetization, $m = M/M_s$, where M is the magnetization and M_s is the saturation magnetization at infinite field, and $h = H/H_a$, where H is the applied magnetic field and H_a is the anisotropy field of the material. Subsequent modifications [2] have included the effect of interactions in the model. Unfortunately, the SW model has no analytic solution, so the calculation of the SW function requires the numerical integration of the m vs. h curves for a distribution of particle orientations, where each individual $m_i(h)$ curve is obtained by minimizing the energy equations for discrete values of h . In real systems, the assumption of coherent rotation invariably fails in the second quadrant, where either domain wall motion or other modes of

demagnetization (such as curling or buckling) provide lower energy paths. Nevertheless, it has been demonstrated [2] that the $M(H)$ curves of hard magnetic materials can be well described by a five-parameter fit with M_s , H_a , an interaction parameter (demagnetization factor $\bar{\gamma}$), and the mean H_S and width ΔH_S of a switching field distribution (SFD). Furthermore, since the SW assumptions are generally valid for the fitting of first quadrant demagnetization curves, such fits yield accurate values of M_s and H_a . This is important in determining a detailed dependence of M_s on temperature T or composition c from experiment, since M_s is often approximated by M_{max} measured at the highest field H_{max} . Since $H_a(T)$ is a function of temperature T , this results in an additional factor in $M(T)$. The same is true when the dependence of M_s on composition is being investigated in an alloy.

While the calculation of the SW dependence $m(h)$ is straightforward, using the tabulated values to fit experimental data is cumbersome [30–33]. The utility of the model can be greatly enhanced by an analytic parameterization of the SW function $m(h)$, so that experimental data can be fitted easily. The SW data [2] was calculated to a precision of 7 significant digits in m for steps of 0.001 in $h \in [-20, 20]$, with known exact values of $m = \pm 1$ at $h = \pm\infty$ and $m(0) = 0.5$, see Table I. The resulting numerical dependence $m(h)$ is then parametrized piecewise by three analytical functions with domains at $h \in [-2, -1]$, $[-1, 2]$, and $[2, +\infty)$, see Fig. 1, and by two inverse analytical functions $h_{\pm}(m)$.

The SW model predicts a kink in the second derivative d^2m/dh^2 at $h = \pm 2$, which is well reproduced by the functions m_1 and $m''_{(2)}$, see Appendix.

PARAMETRIZATION

Direct $m(h)$

We approximate $m(h)$ by 3 analytic functions (Fig. 1):

$$m(h) = \begin{cases} m_1(h), & h \in [2, +\infty); \\ m_2(h), & h \in [-1, 2]; \\ m_3(h), & h \in [-2, -1]. \end{cases} \quad (1)$$

We denote $m_0 \equiv m(-1) \approx -0.05284686$, see Table I. The whole hysteresis loop can be constructed using the inversion symmetry, which transforms $m(h) \rightarrow -m(-h)$; for example,

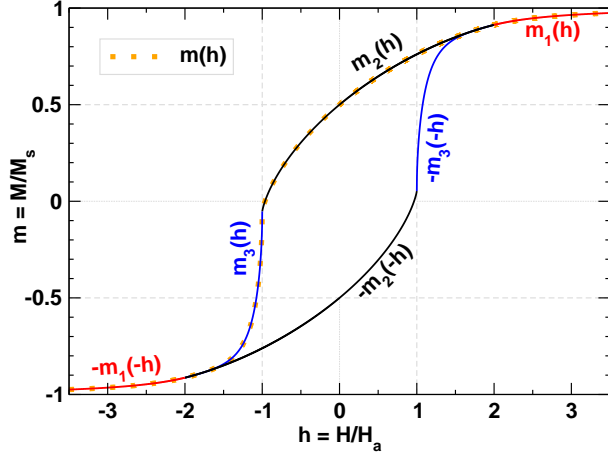


FIG. 1. Piecewise parameterization of the SW hysteresis loop (orange dots) by functions m_1 , m_2 , and m_3 (colored lines).

$m(h) = -m_1(-h)$ at $h \leq -2$. At $h = -1$, the first derivative dm/dh is discontinuous and infinite for m_3 , but $(m_3(h) - m_0)^2$ has a finite slope for all $h \in [-2, -1]$, and we fit this squared function. At $h = 2$, there is a well-known kink in the second derivative d^2m/dh^2 , experimentally observed using the singular point detection techniques [34].

Using machine learning, we perform a piecewise least-squares (LS) fit of the following functions (with coefficients in Table II):

$$\begin{aligned} m_1(h \geq 2) &= \frac{1 + \sum_{n=1}^3 c_n h^{-2n}}{1 + d_1 h^{-2}}, \\ m_2(-1 \leq h \leq 2) &= \frac{0.5 + \sum_{n=1}^6 c_n h^n}{1 + d_1 h + d_2 h^2}, \\ m_3(-2 \leq h \leq -1) &= m_0 + \left[\frac{\sum_{n=1}^3 c_n (-h-1)^n}{1 + \sum_{k=1}^3 d_k (-h-1)^k} \right]^{1/2} \end{aligned} \quad (2)$$

These functions return $m_1(\infty) \equiv 1$, $m_2(0) \equiv 0.5$, and $m_3(-1) \equiv m_0$, see Fig. 1 and Table I. Each function is accurate within its domain, see Appendix.

TABLE I. Values of $m(h)$ and $\overline{\cos \phi}$ from SW [1].

h	$m(h)$	SW [1]
$-\infty$	-1	-1
-1	-0.05284686	-0.052631
0	0.5	0.5
1	0.7607696	0.760770
2	0.9129751	0.9130
3	0.9645663	0.9646
4	0.9809153	0.9809
∞	1	1

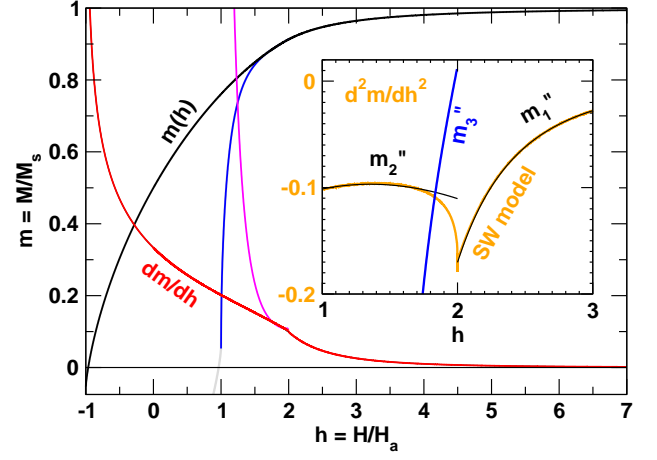


FIG. 2. The SW model (increasing grey $m(h)$ lines), its first (decreasing orange dm/dh in the plot), and second derivatives (orange d^2m/dh^2 lines in the inset), and our approximation by the analytic functions: black m_1 and m_2 , blue $-m_3$, as well as their first (decreasing, same scale, red m'_1 and m'_2 , pink $-m'_3$ lines) and (inset) second derivatives (black m''_1 and m''_2 , blue $-m''_3$ lines). Except for the second derivatives (inset), the SW model and the analytic functionals are indistinguishable, thus most of the gray and orange lines (SW model) are covered by the approximating lines.

Inverse $h(m)$

We also parametrize the inverse function by

$$h(m) = \begin{cases} h_+(m > m_0), & h \in [-1, +\infty); \\ h_-(m \leq m_0), & h \in (-\infty, -1]. \end{cases} \quad (3)$$

A single analytical function $h_+(m)$ in the first quadrant ignores a kink in d^2m/dh^2 at $h = 2$, but covers both m_2 and m_1 . Similarly, $h_-(m)$ is the inverse function for both $-m_1(-h)$ and $m_3(h)$, see Fig. 1.

First, we map $h \in (-\infty, +\infty)$ onto $y \in [0, 1]$ using the transformation $y = 1/[(h+1)^2 + 1]$, and piecewise fit $y(m)$ by two rational functions: one increasing and one decreasing. Next, we substitute those into the inverse transformation $h =$

TABLE II. Coefficients of eqs. 2 and accuracy of the fit: least-squares fit error χ^2 , Theil U, and correlation (C) coefficients.

	m_1	m_2	m_3
c_1	18.2445	1.20029	2.90821
c_2	-5.96049	0.854124	10.1974
c_3	-3.1374	0.116601	-5.12248
c_4	-	-0.031271	-
c_5	-	0.0045254	-
c_6	-	-0.00176557	-
d_1	18.5187	1.73361	4.01935
d_2	-	0.739904	13.3217
d_3	-	-	-7.55852
χ^2	5×10^{-7}	3×10^{-6}	2×10^{-4}
U	5×10^{-6}	4×10^{-5}	1×10^{-3}
C	1.000000	1.000000	0.999995

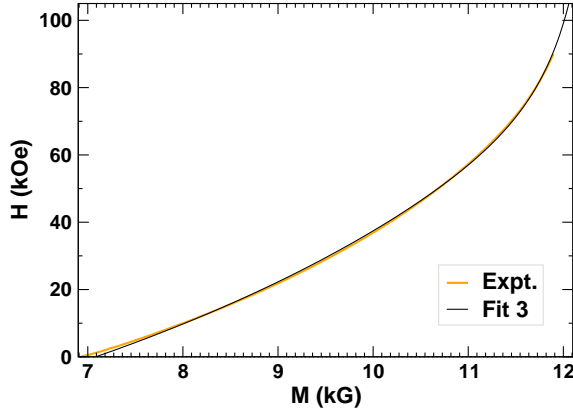


FIG. 3. Experimental data (Expt., orange), fitted (Fit 3, black line) by 3-parameter eq. 5 at $H > 0$.

$-1 + \text{sqr}t(\text{abs}(-1 + 1/y))$, where $\text{sqr}t(x) = \sqrt{x}$ is the square root and $\text{abs}(x) = |x|$ is the absolute value (needed only near $h = -1$). We get

$$h_{\pm}(m) = -1 + \left| -1 + \frac{1 + \sum_{n=1}^5 c_n(m \mp 1)^n}{\sum_{k=1}^5 d_k(m \mp 1)^k} \right|^{1/2} \quad (4)$$

with coefficients in Table III. Here h_{\pm} is expanded in terms of $(m - 1)$. The error in $y[h(m)]$ with $h_{\pm}(m)$ approximated by eq. 4 is below 6×10^{-4} .

APPLICATION

Experiment. The magnetic hysteresis loop was measured for the ribbons of an Ames rare-earth magnetic alloy. To prepare the ribbons, ingots with composition $(\text{Nd}_{0.80}\text{Pr}_{0.20})_2\text{Fe}_{14}\text{B}$ were prepared by arc melting materials of constituent elements in argon atmosphere. Melt spun ribbons were prepared by inductively melting the ingots in quartz crucibles and ejecting the melt onto a single copper wheel at 30 m/s surface velocity through a 0.8 mm orifice.

TABLE III. Coefficients of eqs. 3, see Table II caption.

	h_{+}	h_{-}
c_1	-16.0382	-9.14903
c_2	33.7616	61.4734
c_3	106.516	-336.135
c_4	91.6034	0.290317
c_5	-	18813.8
d_1	-2.59778	4.55815
d_2	0.782093	0.577252
d_3	-43.4887	-357.282
d_4	-52.8431	209.511
d_5	-41.8217	18676.5
χ^2	7×10^{-5}	0.0001
U	0.0004	0.0005
Corr.	1.000000	1.000000

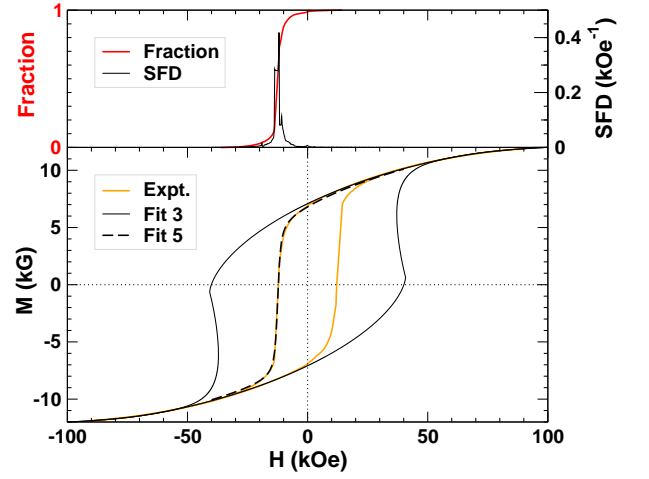


FIG. 4. (Lower) Experimental $M(H)$ data (Expt., orange lines), its 3-parameter fit (Fit 3, solid black lines) by the theoretical curves with demagnetization (eq. 5), and 5-parameter fit (Fit 5, dashed black line) with SFD approximated by eq. 6. (Upper) A fraction of the reversed magnetization (left scale, red) and its derivative (SFD: right scale, black).

Melt spinning was performed in 1/3 atmosphere of high purity He gas. The as-spun ribbons were crystallized by heat treatment at 700°C for 15 min in 1/3 ultra-high purity argon atmosphere. Magnetic hysteresis loop was measured at 300 K in a Quantum Design vibrating sample magnetometer with maximum applied magnetic field of 90 kOe.

Analysis. Eq. 4 can be used to fit a measured data at $H > 0$, taking into account demagnetization:

$$H(M) = H_a h_{+}(M/M_s) - \bar{\gamma} M, \quad (5)$$

where $\bar{\gamma} = \gamma/4\pi$ is a demagnetizing factor. Using a sufficiently large initial guess of M_s to avoid a singularity of $H(M)$ at $M = M_s$, we fit experimental $H(M)$ data at $H > 0$ by 3 parameters (H_a , M_s , $\bar{\gamma}$) in eq. 5.

The result of fitting the measurements at $H > 0$ by eq. 5 is in Fig. 3. We find $H_a = 41.55$ kOe, $M_s = 12.54$ kG, and $\bar{\gamma} = 1.2$.

Due to the switching field, demagnetization data deviates from the SW model (or its parametrization) at $H < 0$. A fraction of the reversed magnetization can be approximated by a sigmoid curve $S(x)$ with two parameters (H_S and ΔH_S) in the argument $x = (H - H_S)/\Delta H_S$.

We use $S_L(x) = \frac{1}{2}(L(x) + 1)$ with the classical Langevin function $L(x) = \coth(x) - 1/x$. Its first derivative is a bell-shaped curve:

$$\begin{aligned} S'_L(H) &\equiv \frac{dS_L}{dH} = \frac{1}{2} \frac{dL}{dx} \frac{dx}{dH} = \\ &= \frac{1}{2 \Delta H_S} \left[1 - \coth^2 \left(\frac{H - H_S}{\Delta H_S} \right) + \left(\frac{\Delta H_S}{H - H_S} \right)^2 \right] \end{aligned} \quad (6)$$

Comparing the upper branch of the experimental $M(H)$ data to the two branches $[m(h)$ and $-m(-h)]$ of the

parametrized SW model, we get a fraction of the reversed magnetization, see Fig. 4. By fitting it to S_L , we get $H_S = -12.44$ kOe and $\Delta H_S^L = 0.484$ kOe. Its derivative is the switching field distribution (SFD), which can be approximated by eq. 6.

SUMMARY

We have provided a convenient analytic approximation for the Stoner-Wohlfarth model [1], suitable for quick and easily computations. We applied it to the measured magnetic hysteresis loop and fitted the experimental data by 5 parameters: M_s , H_a , $\bar{\gamma}$, H_S , and ΔH_S . Our easy-to-compute analytic functions serve as useful tools for description of magnetic materials, that facilitate materials discovery [11, 35–37].

ACKNOWLEDGMENTS

We thank Professors Ivan I. Oleynik and Duane D. Johnson for inspiration and advising. This work was supported by the U.S. Department of Energy, Office of Basic Energy Sciences, Division of Materials Science and Engineering. The research was performed at the Ames Laboratory, which is operated for the U.S. DOE by Iowa State University under contract DE-AC02-07CH11358.

Analysis of $m(h)$ fit and its derivatives

The fitted function $m(h)$ and its derivatives are shown in Fig. 2. Difference between $m(h)$ and its fit by the analytic functions m_n ($n = 1, 2, 3$) from eq. 2 is within the numeric noise. The first derivative of m_n is indistinguishable from dm/dh for the model. The inset in Fig. 2 shows that d^2m/dh^2 is reproduced well at $h > 2$ or $h < 1.7$, but not at $h = 2 - \delta$. The 2nd derivative of m_1 (at $h \geq 2$) coincides with the model, while d^2m_2/dh^2 deviates at $h = 2 - \delta$ for $0 \leq \delta < 0.3$, and the 2nd derivative of $-m_3(-h)$ (blue line in Fig. 2 inset) has a larger deviation near $h = 2$.

The function $m(h)$ itself and its first derivative are reproduced very well everywhere, hence the lines for the SW model and its analytic approximation are indistinguishable in Fig. 2. The function $m_1(h)$ and its derivatives are as good as the tabulated values of $m(h)$ at $h \geq 2$. The largest error (calculated as a deviation from $m(h)$) at a given h is 3×10^{-5} for m_1 at $h = 2$ (it is $< 1 \times 10^{-5}$ for $h > 2.537$ and $< 1.34 \times 10^{-5}$ for $h > 2.066$); 0.001 for m_3 at $h=0$ (< 0.0005 at $0.12 < h < 1$); and 0.0008 for m_2 at $h = -1$ (0.0001 at $h=2$, and $\leq 1 \times 10^{-4}$ at $-0.986 < h \leq 2$).

The first derivative at $h = 2$ is $m'(2) \equiv dm/dh|_{h=2} = 0.09869$ for the model. The error in $m'(2)$ constitutes 0.00037 for m'_1 , 0.003 for m'_2 , and 0.01 for m'_3 . This error in dm/dh is the largest for m'_1 and m'_3 , while dm_2/dh has a smaller error

≤ 0.001 at $-0.8 < h < 1.9$, but an expectedly large error exceeding 0.01 near $h = -1$.

The second derivative $m''_1 \equiv d^2m_1/dh^2$ reproduces the model correctly in the whole domain of m_1 at $h \in [2, +\infty)$, see Fig. 2 inset. However, m''_2 and m''_3 deviate from the model at $h = 2 - \delta$, where $0 \leq \delta < 0.3$. At $h = 2$, this deviation reaches 0.006 for m''_1 , 0.06 for m''_2 , and 0.19 for m''_3 second derivative, where $m''(2) \equiv d^2m/dh^2|_{h=2} \approx -0.18$ for the model, see Fig. 2 inset. If needed, the second derivative d^2m/dh^2 at $-1 < h \leq 2$ can be directly approximated by eq. (7):

$$m''_{(2)} = -0.303321 (h+1)^{-1} - 0.156365 - 0.049342 h + 0.0893185 h^2 - 0.0458726 h^3 + 0.0118055 h^4 + 0.148387 (2-h)^{1/2} + 0.0524192 (2-h)^{1/4},$$

which is accurate even at $h = 2 - \delta$. The function $m_{(2)} \equiv \int \int m''_{(2)}$, obtained by double integration of $m''_{(2)}(h)$ at $-1 < h \leq 2$, contains roots and a logarithm, which are slower to compute.

Equations 2 and 7 provide accurate analytic expressions for $m(h)$ function and its 1st and 2nd derivatives (a luxury, not offered by DLN), while the inverse function $h(m)$ in eq. 4 facilitates a fit of experimental data.

* zarkev@ameslab.gov

† nlebedim@ameslab.gov

- [1] E. C. Stoner and E. P. Wohlfarth, Philosophical Transactions of the Royal Society A **240**, 599 (1948).
- [2] R. W. McCallum, Journal of Magnetism and Magnetic Materials **292**, 135 (2005).
- [3] N. A. Zarkevich, Complexity **11**, 36 (2006).
- [4] G. Pizzi, A. Cepellotti, R. Sabatini, N. Marzari, and B. Kozinsky, Computational Materials Science **111**, 218 (2016).
- [5] J. E. Saal, S. Kirklin, M. Aykol, B. Meredig, and C. Wolverton, JOM **65**, 1501 (2013).
- [6] Y. Zhang and C. Ling, npj Computational Materials **4**, 25 (2018).
- [7] P. Raccuglia, K. C. Elbert, P. D. F. Adler, C. Falk, M. B. Wenny, A. Molloy, M. Zeller, S. A. Friedler, J. Schrier, and A. J. Norquist, Nature **533**, 73 (2016).
- [8] N. A. Zarkevich and D. D. Johnson, Phys. Rev. Lett. **92**, 255702 (2004).
- [9] N. A. Zarkevich and D. D. Johnson, Phys. Rev. B **67**, 064104 (2003).
- [10] N. A. Zarkevich, D. D. Johnson, and A. V. Smirnov, Acta Materialia **50**, 2443 (2002).
- [11] N. A. Zarkevich, D. D. Johnson, and V. K. Pecharsky, Journal of Physics D: Applied Physics **51**, 024002 (2017).
- [12] N. A. Zarkevich and D. D. Johnson, Phys. Rev. B **93**, 020104 (2016).
- [13] N. A. Zarkevich and D. D. Johnson, Surface Science **591**, L292 (2005).
- [14] G. J. Xu, N. A. Zarkevich, A. Agrawal, A. W. Signor, B. R. Trenhaile, D. D. Johnson, and J. H. Weaver, Phys. Rev. B **71**, 115332 (2005).
- [15] N. A. Zarkevich and D. D. Johnson, Phys. Rev. Lett. **100**, 040602 (2008).

- [16] N. A. Zarkevich, T. L. Tan, and D. D. Johnson, Phys. Rev. B **75**, 104203 (2007).
- [17] N. A. Zarkevich, T. L. Tan, L.-L. Wang, and D. D. Johnson, Phys. Rev. B **77**, 144208 (2008).
- [18] N. A. Zarkevich, E. H. Majzoub, and D. D. Johnson, Phys. Rev. B **89**, 134308 (2014).
- [19] N. A. Zarkevich and D. D. Johnson, J. Chem. Phys. **142**, 024106 (2015).
- [20] N. A. Zarkevich and D. D. Johnson, J. Alloys Compd. **802**, 712 (2019).
- [21] N. A. Zarkevich, L.-L. Wang, and D. D. Johnson, APL Materials **2**, 032103 (2014).
- [22] N. A. Zarkevich and D. D. Johnson, Phys. Rev. B **91**, 174104 (2015).
- [23] N. A. Zarkevich and D. D. Johnson, J. Chem. Phys. **143**, 064707 (2015).
- [24] N. A. Zarkevich and D. D. Johnson, Phys. Rev. B **97**, 014202 (2018).
- [25] S. V. Vonsovskii, *Magnetism* (Nauka, Moscow, 1971) in Russian. Translated: Wiley (1974), ISBN 047091193X.
- [26] A. G. Ivahnenko and V. G. Lapa, *Kiberneticheskie predskazyvayushchie ustrojstva* (Naukova Dumka, Kiev, 1965) in Russian.
- [27] I. Goodfellow, Y. Bengio, and A. Courville, *Deep Learning* (MIT Press, 2016).
- [28] S. Russell and P. Norvig, *Artificial Intelligence: A Modern Approach*, 3rd ed. (Pearson, 2016).
- [29] A.G. Stoletov, Lon. E. Dublin Phil. Mag. J. Sci. **45**, 40 (1873), translated from Pogg. Ann. 144, 439–463 (1871). Presented before the Moscow Mathematical Society on 20 Nov (2 Dec) 1871.
- [30] W. Tang, K.W. Dennis, Y.Q. Wu, M.J. Kramer, I.E. Anderson, and R.W. McCallum, IEEE Trans. Magn. **40**, 2907 (2004).
- [31] M. Huang, D. Wu, K.W. Dennis, J.W. Anderegg, R.W. McCallum, and T.A. Lograsso, J. Phase Equilib. Diffusion **26**, 209 (2005).
- [32] S.H. Song, D.C. Jiles, J.E. Snyder, A.O. Pecharsky, D. Wu, K.W. Dennis, T.A. Lograsso, and R.W. McCallum, J. Appl. Phys. **97**, 10M516 (2005).
- [33] A. O. Pecharsky, Y. Mozharivskyj, K. W. Dennis, K. A. Gschneidner, R. W. McCallum, G. J. Miller, and V. K. Pecharsky, Phys. Rev. B **68**, 134452 (2003).
- [34] F. Bolzoni and R. Cabassi, Physica B **346–347**, 524 (2004).
- [35] H. Yibole, A. Pathak, Y. Mudryk, F. Guillou, N. A. Zarkevich, S. Gupta, V. Balema, and V. K. Pecharsky, Acta Materialia **154**, 365 (2018).
- [36] H. N. Bez, A. K. Pathak, A. Biswas, N. A. Zarkevich, V. Balema, Y. Mudryk, D. D. Johnson, and V. K. Pecharsky, Acta Materialia **173**, 225 (2019).
- [37] A. Biswas, A. K. Pathak, N. A. Zarkevich, X. Liu, Y. Mudryk, V. Balema, D. D. Johnson, and V. K. Pecharsky, Acta Materialia **180**, 341 (2019).